Journal of Solid State Chemistry **147,** 390–398 (1999)
Article ID jssc.1999.8392, available online at http://www.idealibrary.com on IDEAL®

Hydrothermal Synthesis, Structural Characterization, and Physical Properties of a New Mixed Valence Iron Phosphate, $SrFe_3(PO_4)_3$

Michael B. Korzenski and Joseph W. Kolis[1]

Department of Chemistry, Clemson University, Clemson, South Carolina 29634-1905

and

Gary J. Long

Department of Chemistry, University of Missouri–Rolla, Rolla, Missouri 65409-0010

Received October 29, 1998; in revised form May 11, 1999; accepted May 24, 1999

DEDICATED TO JEAN ROUXEL

A new mixed valence Fe(II/III) phosphate, $SrFe_3(PO_4)_3$, has been synthesized hydrothermally and structurally characterized by single-crystal X-ray diffraction, EDAX, magnetic susceptibility, Mössbauer, infrared and diffuse reflectance spectroscopies, DTA, and bond valence sum calculations. The compound crystallizes in the orthorhombic space group *I*mma (No. 74) with $a = 10.452(3)$, $b = 13.429(3)$, $c = 6.528(2)$ Å, $V = 916.3(4)$ Å^3 and $Z = 4$ with $R/R_w = 0.0207/0.0307$. The structure consists of a complex low-dimensional framework constructed of FeO_6 octahedra and PO_4 tetrahedra that form 2D channels in which the strontium ions are located. The framework contains two simple building blocks: rigid columns of edge-sharing $Fe_2P_2O_{14}$ units and zigzag chains of alternating PO_4–FeO_6–PO_4 units, both of which run parallel to the *b* direction. This linkage forms intersecting channels which run parallel to the *a* and *b* axes. The divalent strontium cations reside within these channels and create openings in the *ab* plane with dimensions of 6.903(4) and 7.469(4) Å, respectively. These openings can easily accommodate both small and large monovalent or divalent cations, as demonstrated by several cation exchange reactions. The Mössbauer spectral parameters are consistent with the structure and reveal the presence of mixed valent octahedral iron(II) and iron(III) sites in the expected two to one ratio. The quadrupole splittings observed for both iron sites are very large as is expected for the very asymmetric coordination environments found for each iron site. © 1999 Academic Press

INTRODUCTION

Considerable attention has been devoted to preparing new porous transition metal phosphates with both the shape selectivity of a zeolite and the thermal and chemical stability of a metal oxide framework (1). Transition metals can play an important role in microporous frameworks by providing active catalytic sites while retaining the spatial selectivity of the framework. Transition metal centers also facilitate many chemical reactions such as redox chemistry, free-radical chemistry, and photochemical reactions. Therefore, with microporous transition metal phosphates, a whole new class of highly active catalysts may be isolated (2, 3).

Hydrothermal synthesis has been used over the years to grow large, high-quality, single crystals of industrially important materials such as α-quartz (4) and potassium titanylphosphate (KTP) (5). More recently we have been exploring, as a viable alternative in materials synthesis, the potential of supercritical fluids as a synthetic tool for the preparation of new solid-state materials (6). We started using relatively high temperature hydrothermal fluids to isolate new transition metal phosphates. With only a few exceptions (7, 8), very few groups have investigated the synthesis of metal phosphates near 647 K and 221 atm, the supercritical region of water. Although a large number of transition metal phosphates have been prepared hydrothermally, most reactions were generally performed between 370 and 470 K (2, 9). We find that if reactions are performed at high temperatures (550–650 K), a wide variety of new phases can be isolated (10, 11).

Iron phosphates in particular have been shown to possess a rich structural chemistry due both to the ability of iron to adopt multiple oxidation states (+2/+3), and their tendency to form complex octahedral-tetrahedral frameworks of edge- and vertex-sharing MO_6 and PO_4 units. We have investigated the alkaline-earth Fe–P–O system and herein report the isolation and characterization of a new strontium

[1]To whom correspondence should be addressed. E-mail: kjoseph@clemson.edu.

0022-4596/99 $30.00

iron phosphate, $SrFe_3(PO_4)_3$, a compound containing mixed valent iron, and which has structural similarities to both $NaV_3(PO_4)_3$ (12) and α-$CrPO_4$ (13).

EXPERIMENTAL

Synthesis

The starting material $SrHPO_4$ was prepared by adding a stoichiometric amount of H_3PO_4 to a solution of $Sr(OH)_2$ at room temperature followed by filtration and washing of the precipitate with water. A mixture of 0.0405 g (2.2×10^{-1} mmol) of $SrHPO_4$ and 0.0475 g (6.6×10^{-1} mmol) of FeO (molar ratio of Sr : Fe = 1 : 3) were combined in a solution of 0.2 ml of 85% H_3PO_4 and 0.5 ml of distilled water. The reaction mixture was sealed inside an evacuated quartz ampoule with an internal volume of 1.5 ml and heated at 648 K for 3 days followed by cooling, over a period of 2 h, to room temperature. The product consisted of black rectangular-shaped crystals in 91% yield (based on iron) and was determined to be $SrFe_3(PO_4)_3$. It was filtered and washed with water and acetone repeatedly, and dried in an oven at 335 K for 1 h. Qualitative elemental analysis on single-crystal samples using EDAX indicated the presence of Sr, Fe, and P with no significant impurity heavier than F. Attempts to prepare $SrFe_3(PO_4)_3$ by solid-state methods were undertaken by employing three different reactions varying only in the identity of the starting materials. The first reaction consisted of heating an intimate mixture of $SrCO_3$, FeO, and P_2O_5 (molar ratio 2 : 6 : 3) in an alumina boat in air at 673 K for 6 h to drive off the volatile decomposition products, CO_2, NH_3, and H_2O, whereafter it was heated with successive heating cycles of 1173 and 1373 K for two days, respectively, followed by regrinding after each heating. The second and third reactions were undertaken using the identical heating procedure but with mixtures of $SrCO_3$, FeO, and $(NH_4)_2HPO_4$ (molar ratio 1 : 3 : 3) and SrO, FeO, and $(NH_4)_2HPO_4$ (molar ratio 1 : 3 : 3). All three reactions led to a pale orange and white biphasic mixture of $Fe_3(PO_4)_2$ (14) and $Sr_2P_2O_7$ (15), respectively, as determined by X-ray powder diffraction. It is not surprising that synthesis by high-temperature ceramic methods leads to exclusively Fe(II) products, but it does indicate that the title compound cannot be prepared over a wide range of conditions.

Characterization Methods

An X-ray powder diffraction pattern of the title compound was obtained at room temperature with a 0.25°/min step scan using a Scintag XDS 2000 θ–2θ powder diffractometer and Cu$K\alpha$ radiation ($\lambda = 1.5406$ Å). The Mössbauer spectra were measured at 78 and 295 K on a conventional constant acceleration spectrometer which utilized a room-temperature rhodium matrix cobalt-57 source, and was calibrated at room temperature with γ-iron foil. The resulting spectra were least-squares fit with symmetric quadrupole doublets with Lorentzian lineshapes. No indication of any long-range magnetic order was observed in the spectra. The magnetic susceptibility was measured using a Quantum Design SQUID MPMS-5S magnetometer. Ground single-crystal samples ($\approx$12.7 mg) were placed in a gel capsules ample holder which was suspended in a plastic drinking straw. The temperature and field dependence of the susceptibility of the container had been previously determined and their effect on the total susceptibility was negligible. The measurement was performed at 1.0 T over the 2–300 K temperature range. The thermal stability of $SrFe_3(PO_4)_3$ was examined with a DuPont Instruments Thermal Analyst 2000 equipped with a high temperature 1600 DTA cell adaptor. The ground crystals ($\approx$15 mg) were heated from 298 to 1273 K at 5°/min and then isothermed for 5 min, followed by cooling at 5°/min to room temperature. After the DTA measurements, the sample was examined by powder X-ray diffraction. The optical bandgap of a powder sample of $SrFe_3(PO_4)_3$ was determined from room temperature diffuse reflectance measurements, between 200 and 2500 nm, on a Schimadzu UV3100 spectrophotometer equipped with an integrating sphere. Barium sulfate was used as the reflectance standard. The reflectance data were converted to relative absorption units using the Kubelka–Munk function (16), $\alpha/S = (1 - R)^2/2R$, where R is the reflectance at a given wavelength, α is the absorption coefficient, and S is the scattering coefficient. The infrared absorption spectra of a single crystal was studied between 1200 and 400 cm^{-1} on a Nicolet Magna-IR Spectrometer 550 with a Spectra Tech IR-Plan Laboratory Microscope single crystal attachment. The energy dispersive X-ray analysis (EDAX) of a single crystal was obtained using a JEOL JSM-IC 848 scanning microscope equipped with a Princeton Gamma Tech (PGT) PRISM detector. For ion-exchange experiments, approximately 50 mg of $SrFe_3(PO_4)_3$ was added to a supersaturated solution of the corresponding MCl_2 salt (where M is Mg^{2+}, Ca^{2+}, and Ba^{2+}) in a 50-ml round bottom flask. The aqueous solution was refluxed for 16 h, filtered, and then washed repeatedly with copious amounts of deionized water and acetone. The powdered sample was then dried in an oven at 333 K for 2 h.

Single-Crystal Structure Determination

A black rectangular-shaped single crystal of $SrFe_3(PO_4)_3$ was mounted on a glass fiber with a minimal amount of epoxy and placed on a Nicolet R3mV sealed tube diffractometer equipped with graphite monochromated Mo$K\alpha$ radiation ($\lambda = 0.71073$ Å). Final unit cell dimensions and the orientation matrix were determined by a least-squares fit of 48 randomly located reflections between 45.63° and 56.43°

in 2θ. Data were collected on an orthorhombic cell at 2–15°/min using the θ–2θ scan mode according to the parameters given in Table 1. Crystal integrity and experimental stability were monitored during the data collection by measuring the intensities of the three standards after every 97 reflections. The intensity data were corrected for Lorentz and polarization effects and an empirical absorption correction based on ψ-scans (17) for six reflections with χ between 60 and 90° was applied to compensate for absorption effects. The crystallographic results are summarized in Table 1 and the atomic coordinates and selected bond distances and angles are listed in Tables 2 and 3, respectively.

On the basis of the lattice parameters, Laue symmetry tests, reflection conditions $hkl: h + k + l = 2n$ and $hk0$: $h, k = 2n$, the possible space group choices for $SrFe_3(PO_4)_3$ were *Imma* and the nonstandard space group *Im*2*a* of the space group *Ima*2. However, on the basis of statistical tests and the successful subsequent structure refinement, the centrosymmetric space group *Imma* was chosen. The space group was confirmed via the MISSYM (18) algorithm within the PLATON (19) program suite. Structure determination and refinement were performed on a Digital VAXstation 4000 using the SHELXTL-PLUS program packages (20) and refined using full-matrix least-squares techniques with scattering factors taken from the source programs. Direct methods were used to locate all heavy atoms and the remaining atoms were found from successive Fourier different maps. All atoms were refined with anisotropic thermal parameters.

TABLE 1
Crystallographic Data for $SrFe_3(PO_4)_3$

Chemical formula	$SrFe_3(PO_4)_3$
Formula weight (g/mol)	540.1
a (Å)	10.452(3)
b (Å)	13.429(3)
c (Å)	6.528(2)
V (Å^3), Z	916.3(4), 4
Space Group (No.)	*Imma* (No. 74)
ρ_{calc} (g/m^3)	3.915
Crystal shape, color,	black, rectangle,
Size(mm)	$0.43 \times 0.11 \times 0.11$
Scan type/Scan range (°)	θ–2θ/$0.68 + 0.35\tan\theta$
2θ min, max (°)	3.5–55.0
Indices	$\pm h,\ \pm k,\ +l$
No. of reflections measured	2298
No. of reflections unique (R_{int})	587, 0.0538
No. of reflections with $I > 2\sigma(I)$	550
No. of parameters	55
Transmission factors	0.56–1.00
Secondary extinction	N/A
Final R(F)[a], R_w (F)[b]	0.0207, 0.0307
Goodness of fit (S)[c]	1.06
Residual (e$^-$/Å^{-3}), max. shift	0.58/ − 0.69; 0.0007

[a] $R = \sum \| F_o| - |F_c \| / \sum |F_o|$.
[b] $R_w = [w\{|F_o| - |F_c|\}^2 / w|F_o|^2]^{1/2}$; $w = 1/[\sigma^2(F) + 0.0005F^2]$
[c] $S = [?(?F_o?_i - ?F_c?_i)/\sigma_i]/(n - m)$; $i = 1$ to n.

TABLE 2
Atomic Coordinates and Thermal Parameters[a] for $SrFe_3(PO_4)_3$

Atom	Wyckoff	x	y	z	U_{eq}
Sr(1)	4*e*	0	1/4	0.6007(1)	0.009(1)
Fe(1)	4*a*	0	0	0	0.006(1)
Fe(2)	8*g*	1/4	0.1324(1)	1/4	0.008(1)
P(1)	8*g*	1/4	−0.0736(1)	1/4	0.006(1)
P(2)	4*e*	0	1/4	0.0954(2)	0.005(1)
O(1)	16*j*	0.1386(2)	0.1200(2)	0.2033(3)	0.008(1)
O(2)	8*h*	0	0.1567(2)	−0.0404(5)	0.008(1)
O(3)	16*j*	0.2899(2)	0.1366(1)	−0.0679(3)	0.010(1)
O(4)	16*j*	0.1167(3)	0.2500	0.2402(4)	0.008(1)

[a] The equivalent isotropic temperature factor, U_{eq}, is defined as $1/3\{\Re_i \Re_j (U_{ij} a_i^* a_j^* a_i \cdot a_j)\}$, where the summations of i and j range from 1 to 3.

RESULTS AND DISCUSSION

Structural Description

The polyhedral unit cell structure of $SrFe_3(PO_4)_3$, as viewed along the (100) direction, is shown in Fig. 1. The

TABLE 3
Selected Bond Distances (Å) and Angles (°) with ESD's for $SrFe_3(PO_4)_3$

		$[FeO_6]$ octahedra	
Fe(1)–O(1)	1.965(2) × 4	Fe(1)–O(2)	2.121(3) × 2
O(1)–Fe(1)–O(2)	94.3(1) × 4	O(1)–Fe(1)–O(1)	180.0(1) × 2
O(2)–Fe(1)–O(1)	85.7(1) × 4	O(1)–Fe(1)–O(1)	85.0(1) × 2
O(1)–Fe(2)–O(1)	95.0(1) × 2	O(2)–Fe(1)–O(2	180.0(1)
O(1)–Fe(2)–O(2)	89.4(1)		
Fe(2)–O(1)	2.134(2) × 2	Fe(2)–O(3)	2.117(2) × 2
Fe(2)–O(4)	2.107(2) × 2	O(1)–Fe(2)–O(4)	104.7(1)
O(3)–Fe(2)–O(4)	94.6(1) × 2	O(1)–Fe(2)–O(1)	68.7(1)
O(3)–Fe(2)–O(1)	93.1(1) × 2	O(4)–Fe(2)–O(1)	169.8(1) × 2
O(3)–Fe(2)–O(3)	176.9(1)	O(4)–Fe(2)–O(3)	83.1(1) × 2
O(1)–Fe(2)–O(3)	89.4(1)	O(4)–Fe(2)–O(4)	82.9(1)
O(1)–Fe(2)–O(4)	104.7(1)		
		$[PO_4]$ tetrahedra	
P(1)–O(1)	1.568(2) × 2	P(1)–O(3)	1.518(2) × 2
O(1)–P(1)–O(1)	100.3(2)	O(1)–P(1)–O(3)	107.8(1) × 2
O(1)–P(1)–O(3)	114.2(1) × 2	O(3)–P(1)–O(3)	112.2(2)
P(2)–O(2)	1.535(3) × 2	P(2)–O(4)	1.543(3) × 2
O(2)–P(2)–O(4)	110.7(1) × 4	O(2)–P(2)–O(2)	109.4(2)
O(4)–P(2)–O(4)	104.5(2)		
		$[SrO_8]$ polyhedra	
Sr–O(2)	2.657(3) × 2	Sr–O(3)	2.681(2) × 4
Sr–O(4)	2.651(3) × 2		

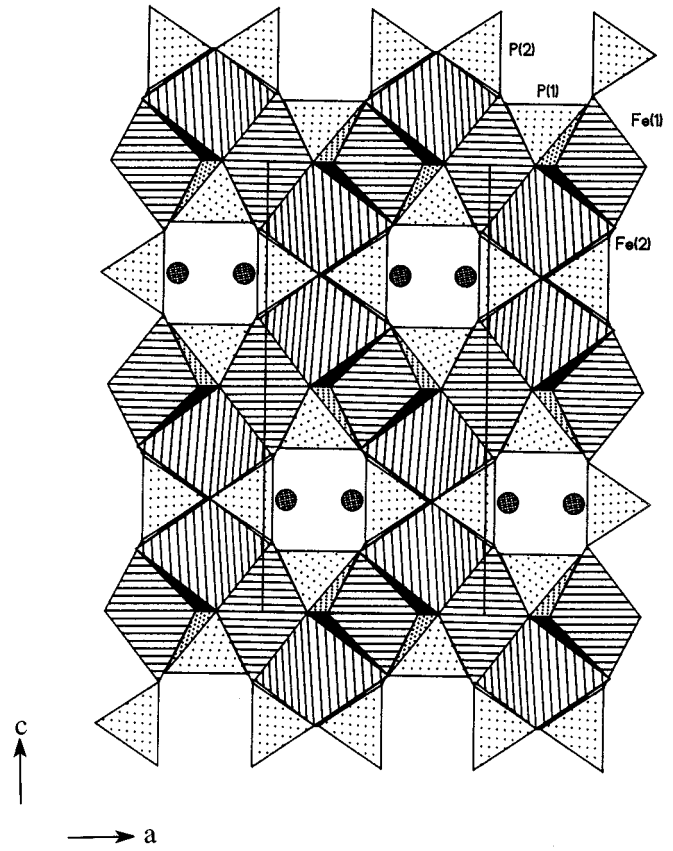

FIG. 1. The polyhedral unit cell structure of $SrFe_3(PO_4)_3$ as viewed down the *a* axis. The FeO_6 octahedra and PO_4 tetrahedra are drawn as lined and dotted patterns, respectively, with strontium atoms depicted as cross hatched spheres.

structure consists of a complex three-dimensional framework constructed of FeO_6 octahedra and PO_4 tetrahedra that form 2D channels in which the strontium ions are located. The framework is composed of two simple building blocks: rigid columns consisting of edge-sharing $Fe_2P_2O_{14}$ units and zigzag chains of alternating PO_4–FeO_6–PO_4 units linked by vertex-sharing O(2) ions, both of which run parallel to the *b* axis (Fig. 2). In the former structural unit, $Fe_2P_2O_{14}$, each Fe(2)O_6 octahedron shares opposite edges with another, symmetry generated, octahedron and P(1)O_4 tetrahedron. The individual units are linked together by the sharing of O(1) and O(4) ions of the phosphate, and this linkage forms intersecting channels which run parallel to the *a* and *b* axes (Fig. 1). The divalent strontium cations reside at the intersection of these channels creating openings in the *ab* plane with dimensions of 6.903(4) and 7.469(4) Å, respectively. These openings can easily accommodate both small and large monovalent or divalent cations, as is observed in cation exchange studies (vide infra).

The Fe(1) atom sits on the origin whereas Fe(2) sits on the 2/*m* site at (1/4, *y*, 1/4). With the exception of O(1) and O(3), which are on general positions, all other atoms are located on special positions. Both Fe atoms are coordinated to six oxygen ions with average Fe–O distances of 2.017(3) and 2.117(3) Å for Fe(1) and Fe(2), respectively, which is typical for related Fe/P/O systems (21). The Fe(1)O_6 octahedra, which make up the zigzag chain, possess a rather regular octahedral geometry with bond angles which range from 85.0(1) to 95.0(1)° and with exactly 180(1)° for the cis and trans angles, respectively. However, the Fe(2)O_6 octahedron

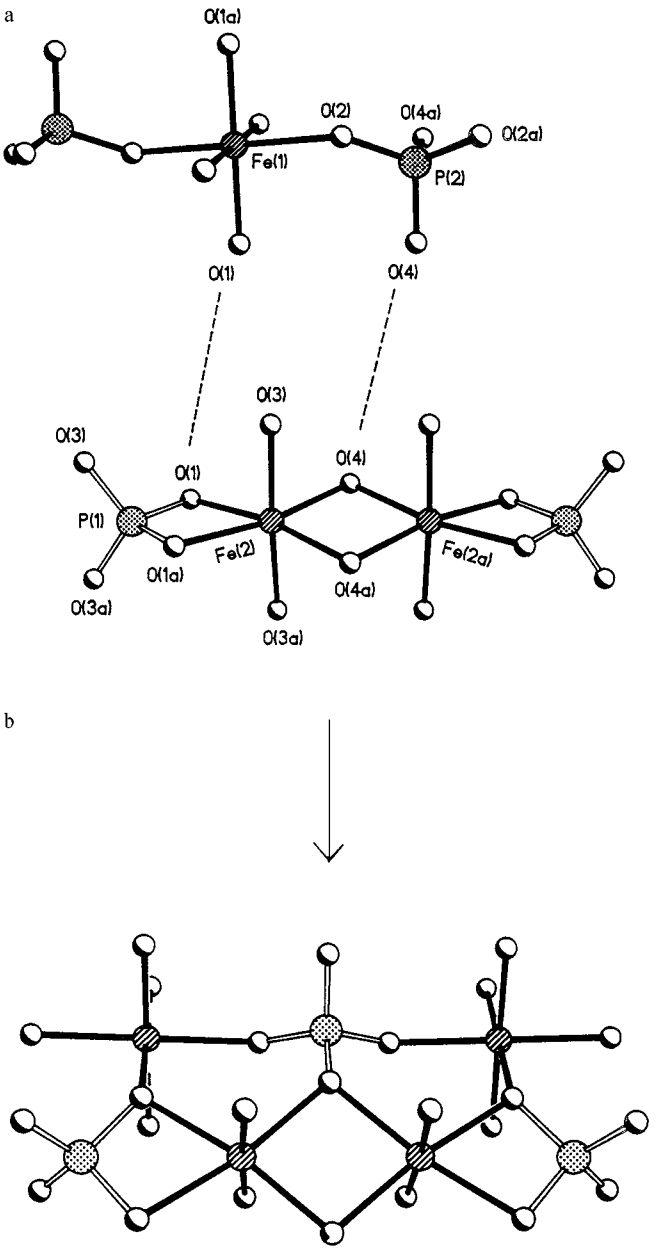

FIG. 2. The two structural units in $SrFe_3(PO_4)_3$ (a) the rigid columns consisting of edge-sharing $Fe_2P_2O_{14}$ units (b) zigzag chains of alternating PO_4–FeO_6–PO_4 units.

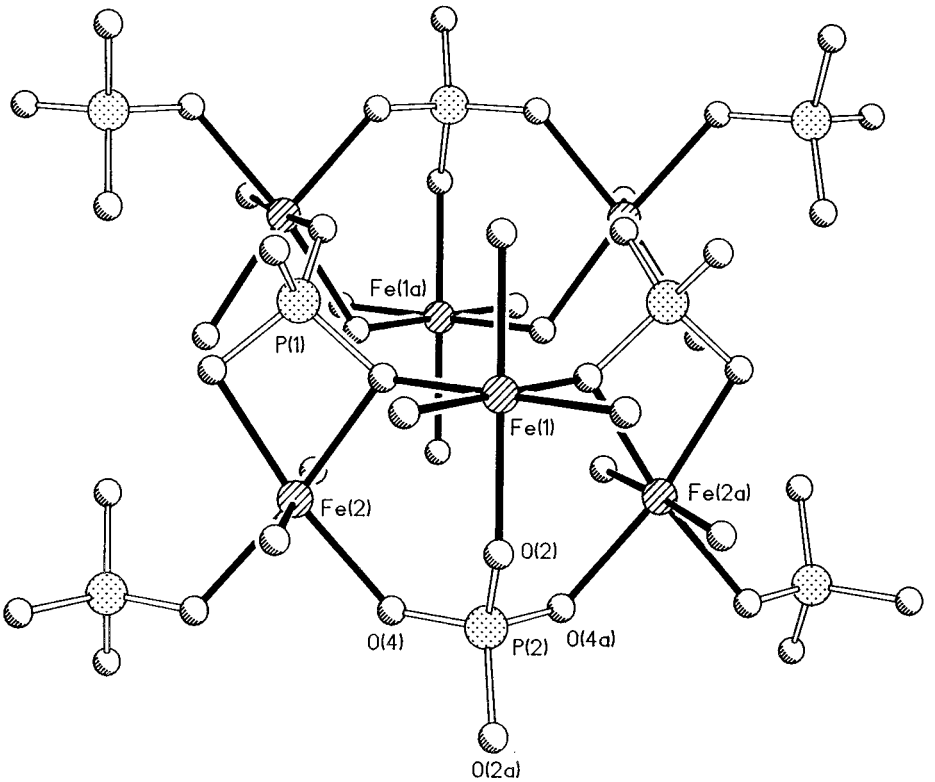

FIG. 3. Phosphate tetrahedra connecting the infinite FeO_6 chains in the c direction.

within the $Fe_2P_2O_{14}$ cluster is very distorted with bond angles that range from 68.7(1) to 94.6(1)° and 169.8(1) to 176.9(1)° for the cis and trans angles, respectively. This distortion is a result of the rigid environment surrounding Fe(2) (Fig. 2). The degree of distortion in the $Fe(2)O_6$ octahedron is more evident when compared to the value of the nearly ideal $Fe(1)O_6$ octahedron obtained from $\Delta = (1/6)\sum((R_i - R_a)/R_a)^2$, where R_i is an individual bond length and R_a is the average bond length (22). This formula yields degrees of distortion of 1.3 ($\Delta = 10^3$) and 2.8 ($\Delta = 10^5$) for Fe(1) and Fe(2), respectively.

P(2) is vertex-shared to Fe(1) and Fe(2) at adjacent oxygen ions O(2) and O(4), respectively. This forms a P(2)–O(2)–Fe(1) linkage that creates linear chains which run parallel to the b axis, and a P(2)–O(4)–Fe(2) linkage which helps hold together the 3D framework along the a axis (Fig. 3). P(1) is interconnected to both Fe(1) and Fe(2) to form linkages in all three axial directions. The strontium ions are located at the intersections of the 2D channels and are coordinated to eight oxygen atoms with distances ranging from 2.651(3) to 2.681(2) Å.

There have been a number of strontium iron phosphate compounds reported previously (23–25), but none possess this structure. However, the structure of $SrFe_3(PO_4)_3$ is related to that observed for $NaV_3(PO_4)_3$, and both compounds are stuffed variants of α-$CrPO_4$, which possesses a similar tunnel framework. Due to the small difference between the ionic radii of Na^+ and Sr^{2+}, and because $NaV_3(PO_4)_3$ and $SrFe_3(PO_4)_3$ both feature the same structural framework, it is not surprising that both these ions can occupy the same crystallographic site. The framework–metal–atom densities (FD) of $SrFe_3(PO_4)_3$ and $NaV_3(PO_4)_3$ are 26.2 M atoms/1000 Å^3 and 26.8 M atoms/1000 Å^3 (M = Metal and P), respectively, as compared with the value of 28.4 M atoms/1000 Å^3 for the more condensed α-$CrPO_4$. These calculated values correlate well with α-$CrPO_4$ considering that it does not contain any alkali or alkaline-earth ion to expand the framework.

Bond valence sum calculations (26) are listed in Table 4 and clearly indicate that the iron atoms and all atoms within the anionic framework are in good agreement with their formal oxidation states. These calculations, along with the observed magnetic moment and the multiplicity of the two crystallographically unique iron sites, suggest that Fe(1) is in the +3 oxidation state and the two Fe(2) atoms are in the +2 oxidation state. This is what would be expected in order to obtain the necessary charge neutrality of the compound. It should be noted that the two trivalent vanadium ions in $NaV_3(PO_4)_3$ must be the crystallographically equivalent of the two Fe(2) ions in $SrFe_3(PO_4)_3$ in order to achieve charge balance, and indeed this appears to be the case (12).

TABLE 4
Bond Valence Sums for Atoms in $SrFe_3(PO_4)_3$

Atom	*d* (Atom–O)	Bond sum[a]
Sr(1)	2.651–2.681	1.81(3)
Fe(1)	1.965–2.121	3.04(5)
Fe(2)	2.107–2.134	2.12(3)
P(1)	1.518–1.568	4.90(8)
P(2)	1.535–1.543	4.94(2)
O(1)	—	2.05(1)
O(2)	—	1.86(5)
O(3)	—	1.88(2)
O(4)	—	1.82(3)

[a]Bond sum $= \exp[r_0 - r)/B]$, where r_0 = empirically determined parameter from Ref. 7, $B = 0.37$, and r = bond distance.

Physical Characterization of $SrFe_3(PO_4)_3$

The X-ray powder diffraction pattern of $SrFe_3(PO_4)_3$ was calculated using the lattice parameters and atomic positions obtained from the single-crystal study, and all the calculated peaks corresponded to the observed pattern. Energy dispersive X-ray analysis (EDAX) on a single crystal qualitatively confirmed the presence of only strontium, iron, and phosphorous in approximately the correct ratios.

Differential thermal analysis of $SrFe_3(PO_4)_3$ revealed two thermal events consisting of a sharp endotherm at 1229.70 K (0.11°C/mg) on the heating curve followed by a sharp exotherm at 1142.64 K (0.32°C/mg) on the cooling curve. The first peak corresponds to a melting transition whereas the second peak corresponds to recrystallization. The large temperature difference between the two peaks is indicative of incongruent melting. This is confirmed by the powder XRD pattern of the heated sample which shows evidence of a two phase mixture of $Sr_2P_2O_7$ and $Fe_3(PO_4)_2$.

The infrared spectrum of $SrFe_3(PO_4)_3$ revealed P–O vibrational frequencies associated with the $[PO_4]^{3-}$ groups (27) as two broad peaks of medium intensity centered at 1090(s) and 990(s) cm^{-1}, along with another band at 550(m) cm^{-1}, which presumably can be assigned to the iron oxygen stretching vibration.

The Mössbauer spectra of $SrFe_3(PO_4)_3$, measured at 78 and 295 K are shown in Fig. 4 and the hyperfine parameters corresponding to the fits shown in this figure are given in Table 5. The fits, which consist of two symmetric quadrupole doublets, are assigned to the two different iron sites in $SrFe_3(PO_4)_3$ on the basis of their relative areas and are clearly consistent with the presence of both high-spin iron(II) and high-spin iron(III). Alternative fits, in which the two component spectral lines at ca. -0.40 mm/s are reversed, give virtually identical misfits. However, the temperature dependencies of the isomer shifts derived from the alternative fits are not as reasonable as those of the fits shown in Fig. 4. The relative areas of the doublets obtained from the least-squares fits agree virtually perfectly with those calculated from the structure and the stoichiometry of the compound, as expected, at 78 K.

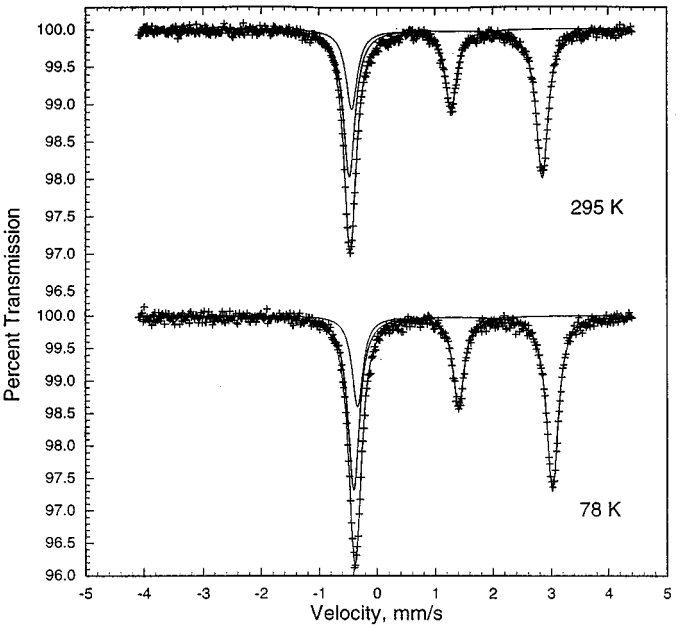

FIG. 4. Mössbauer spectrum of $SrFe_3(PO_4)_3$ at 295 K (upper) and 78 K (lower).

The hyperfine parameters given in Table 5 are completely consistent with the electronic properties of $SrFe_3(PO_4)_3$ and with those obtained from related compounds (28–33). Indeed, very similar spectra to those shown in Fig. 4 have been observed (32) between 295 and 220 K for α-$Fe_2(PO_4)O$, and the 295 K iron(III) isomer shift reported in Table 5 is only slightly smaller than that of the iron(III) site in α-$Fe_2(PO_4)O$ and to the values found in a series of structurally related iron(III) phosphates (31). In contrast, the 295 K iron(II) isomer shift of 1.19 mm/s observed for $SrFe_3(PO_4)_3$ is substantially larger than the 1.06 mm/s

TABLE 5
Mössbauer Spectral Parameters for $SrFe_3(PO_4)_3$

Site	*T*, K	δ[a], mm/s	ΔE_Q, mm/s	Γ, mm/s	% Area, observed	% Area, expected[b]	Abs. Area (%ε) (mm/s)
Fe(1)	295	0.468	1.66	0.235	16.9	16.9	4.08
Fe(2)		1.20	3.37	0.315	55.6	55.5	
Fe(1)	78	0.581	1.74	0.222	16.4	16.1	4.80
Fe(2)		1.32	3.46	0.331	55.5	55.2	

[a]Relative to room temperature α-iron foil.
[b]The percentage area expected on the basis of the stoichiometry and the crystal structure.

value observed in α-$Fe_2(PO_4)O$, presumably because the former compound has a substantially shorter 2.119 Å average iron(II) to oxygen bond distance than the 2.141 Å average distance found (34) in α-$Fe_2(PO_4)O$. It is these very short iron(II) to iron(III) distances that yield an ordering temperature (32) of ca. 220 K in α-$Fe_2(PO_4)O$ as compared to the value of 55 K observed for $SrFe_3(PO_4)_3$, see below. The 1.19-mm/s isomer shift is, however, very similar to that observed (34) for the iron(II) ions in the mixed valent phosphate, $Fe_3(II)Fe_4(III)(PO_4)_6$, and for the divalent Fe(1) site in $Fe_9(PO_4)O_8$ (31).

The quadrupole splittings, ΔE_Q, for the Fe(1) and Fe(2) sites in $SrFe_3(PO_4)_3$ are clearly indicative of iron ions in highly distorted octahedral coordination environments (35, 36). Although quadrupole splittings as large as ca. 4.3 mm/s have been observed (37) for the trigonal prismatic iron(II) site in $Fe_3(P_2O_7)_2$, the observed quadrupole splittings of 3.32 mm/s at 295 K and 3.42 mm/s at 78 K, are, to our knowledge, the largest iron(II) quadrupole splittings observed at a pseudooctahedral iron(II) site in an iron phosphate compound. More specifically, these values are substantially higher than the 2.39 mm/s quadrupole splitting observed (32) at 295 K for α-$Fe_2(PO_4)O$ and the 2.56 mm/s value observed (35) at 300 K for $Fe_3(II)Fe_4(III)(PO_4)_6$. In addition, the observed Fe(1) iron(III) quadrupole splittings of 1.71 mm/s at 295 K and 1.74 mm/s at 78 K, are very large as these quadrupole splittings are typically found in the approximate range of 0.4 to 1.0 mm/s in iron(III) phosphate compounds, one of the largest values being the 0.98 mm/s observed splitting at 295 K for the iron(III) site in α-$Fe_2(PO_4)O$ (32). Although based on only two values, the temperature dependence of the isomer shift and the logarithm of the spectral absorption area are very reasonable. The resulting (38) effective recoil masses of 81 and 74 g/mol for the Fe(1) and Fe(2) sites, are rather high for an ionic compound and indicate the presence of extensive covalence at both iron sites in $SrFe_3(PO_4)_3$, a covalence which is expected for the rather short iron–oxygen bond distances found in this compound. The resulting effective Mössbauer temperatures (38) are 317 and 276 K for the Fe(1) and Fe(2) sites, respectively, a very similar value has been reported (31) for $Fe_9(PO_4)O_8$.

The temperature dependence of the magnetic susceptibility data for $SrFe_3(PO_4)_3$ cooled in zero field, is shown in Fig. 5. The sample displays Curie–Weiss law behavior over the 55 to 300 K temperature range with a Weiss constant of 37.8 K, a value which implies that the dominant interactions between the edge-sharing FeO_6 octahedron are strong and ferromagnetic. This is confirmed by the sharp ferromagnetic transition at the inflection point, T_c, of ca. 55 K. The Curie constant of 10.2 emu K^{-1} per formula unit corresponds to an effective magnetic moment/Fe center of 5.22 μ_B, a value which is between the expected spin-only values of 4.90 and 5.92 μ_B for Fe^{2+} and Fe^{3+}, respectively. This calculated

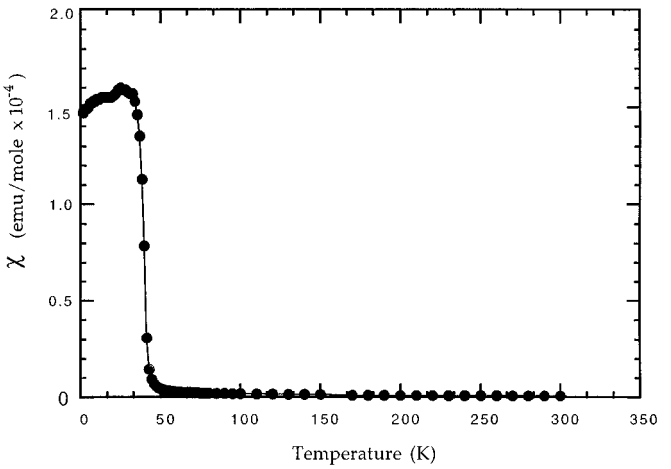

FIG. 5. Plot of magnetic susceptibility as a function of temperature for $SrFe_3(PO_4)_3$.

value is consistent with the assignment of high-spin, mixed-valent Fe^{2+}/Fe^{3+} electronic configurations in octahedral environments in which the contribution from the orbital angular momentum may be increasingly important.

UV-vis diffuse reflectance measurements on ground crystals of $SrFe_3(PO_4)_3$ were obtained between 200 and 2500 nm (6.2–0.5 eV) in order to determine the optical bandgap. In the case of $SrFe_3(PO_4)_3$ the plots of $(absorbance)^2$ and $(absorbance)^{1/2}$ vs energy were compared to determine which plot had a better linear dependence at the absorption edge. The $(absorbance)^2$ vs energy plot yielded a better fit, suggesting that $SrFe_3(PO_4)_3$ possesses a direct bandgap (39). Thus, the bandgap was obtained by determining the inflection point of the first derivative of the reflectance vs energy plot, and gave an optical bandgap of 0.93 eV or 7500 cm^{-1} for $SrFe_3(PO_4)_3$ (Fig. 6). There is also a slightly

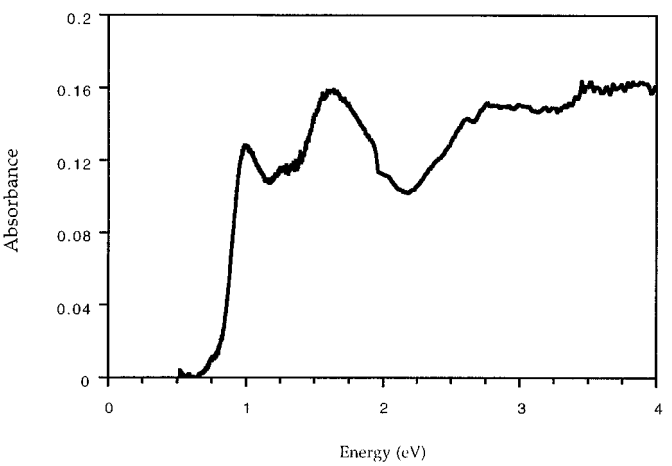

FIG. 6. The optical absorption spectrum of $SrFe_3(PO_4)_3$.

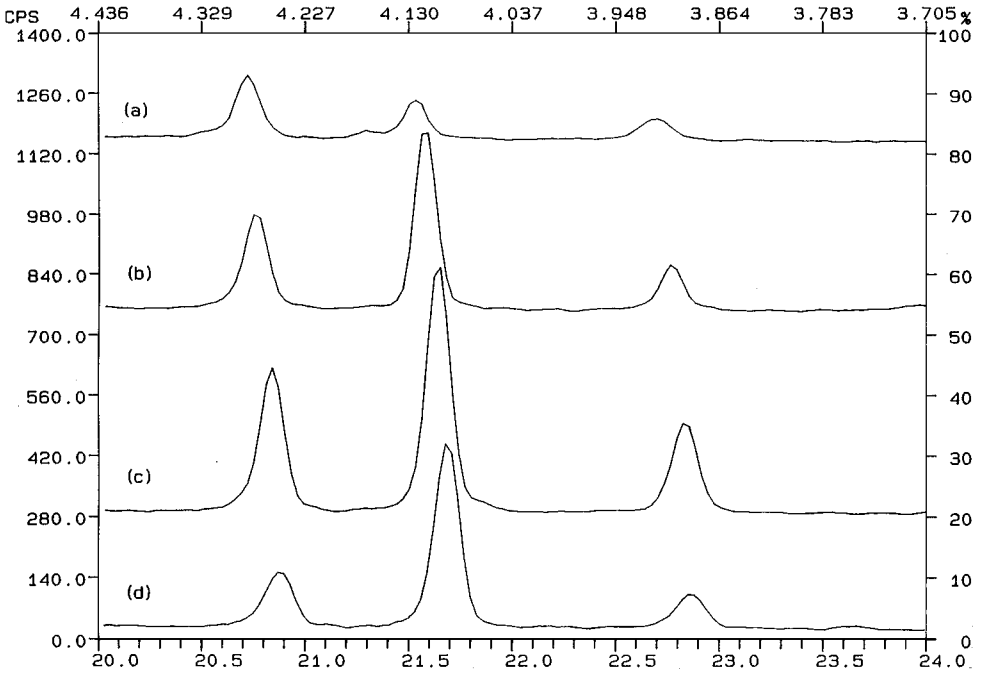

FIG. 7. X-ray powder patterns of the ion exchanged materials emphasizing the 20–24° region , showing peak shifts which indicate the change in unit cell size after ion exchange: (a) $Sr_{(1-x)}(NH_4)_xFe_3(PO_4)_3$, (b) $Sr_{(1-x)}Ba_xFe_3(PO_4)_3$, (c) $SrFe_3(PO_4)_3$, (d) $Sr_{(1-x)}Ca_xFe_3(PO_4)_3$.

smaller transition near 1.6 eV which may be a *d–d* transition of the iron sites.

Ion Exchange

Due to the large two-dimensional channels in $SrFe_3(PO_4)_3$ which contain the strontium ions, $SrFe_3(PO_4)_3$ has the potential for exhibiting ion-exchange properties. Therefore, studies were undertaken to investigate the ion-exchange of the strontium ion with other alkaline-earth cations and ammonium cations. The ion-exchange studies consisted of a 16-h reflux of $SrFe_3(PO_4)_3$ in aqueous solutions of Ca^{2+}, Ba^{2+}, and NH_4^+ cations, followed by X-ray diffraction studies to determine any cell size variations. The results give an indication of partial exchange of the strontium cation in all three cases studied due to shifts in the 2θ values (Fig. 7). Given the *hkl* values calculated from the single-crystal data of the parent phase, $SrFe_3(PO_4)_3$, the lattice parameters of the ion-exchange samples were calculated refining 29 peaks for each sample. The results are listed in Table 6 which reveals either an increase or decrease, as expected, based on the size of the exchanged cation, with an approximately equal expansion along all three axes of the unit cell. The complement the XRD data which confirms that ion-exchange has definitely occurred, energy dispersive X-ray analysis of the powdered samples was obtained, revealing the presence of the exchange cation and the absence of chlorine in all cases. However, a detectable ($>50\%$) amount of strontium was still present in all cases, indicating that only partial ion-exchange had occurred. Unfortunately, the end member compounds could not be obtained so Vegard's law could not be used to determine the degree of cation substitution. This correlates with the observation that attempts to make $MgFe_3(PO_4)_3$, $CaFe_3(PO_4)_3$, and $BaFe_3(PO_4)_3$ hydrothermally were unsuccessful because other phases were formed preferentially. However, it does indicate that the divalent metal ions do exchange to a measurable degree in this material.

CONCLUSIONS

$SrFe_3(PO_4)_3$, a new mixed valence iron phosphate, has been prepared by using hydrothermal techniques and characterized by single-crystal X-ray crystallography, magnetic

TABLE 6
Comparison of Lattice Parameters of Ion-Exchange Compounds

Compound	*a* (Å)	*b* (Å)	*c* (Å)	*V* (Å^3)
$Sr_{1-x}Ca_xFe_3(PO_4)_3$	10.407(5)	13.385(7)	6.5306(5)	909.30(17)
$SrFe_3(PO_4)_3$	10.413(4)	13.406(4)	6.5404(3)	916.13(11)
$Sr_{1-x}Ba_xFe_3(PO_4)_3$	10.438(3)	13.421(4)	6.5519(3)	917.89(10)
$Sr_{1-x}(NH_4)_xFe_3(PO_4)_3$	10.452(3)	13.436(2)	6.5598(6)	921.17(11)

susceptibility, thermal analysis, diffuse reflectance spectroscopy, and Mössbauer spectroscopy. It is structurally similar to both $NaV_3(PO_4)_3$ (12) and α-$CrPO_4$ (13), and the framework can accommodate both small and large alkaline-earth metal ions as shown by ion-exchange experiments. The presence of metal–metal interactions due to the edge-sharing FeO_6 octahedron gives rise to ferromagnetic behavior as observed in the magnetic susceptibility measurements. Numerous other strontium iron phosphates have been reported previously but none with this structure. In addition, the compound is thermally stable to 1100 K but apparently cannot be made by classical dry techniques. These facts illustrate the importance and richness of high-temperature hydrothermal synthesis as a synthetic technique.

ACKNOWLEDGMENTS

Financial support for this research from the National Science Foundation (Grant CHE-9102548 (JWK) and DMR-9521739 (GJL)) is gratefully acknowledged. We also thank the Shiou-Jyh Hwu group for the use of their DTA and Mr. D. Hautot and Dr. O. A. Pringle for assistance in obtaining the Mössbauer spectra. Tables of detailed crystallographic data such as bond angles, figures of cation coordination, and the asymmetric unit are available from the author upon request.

REFERENCES

1. G. Le Flem, *Eur. J. Solid State Inorg. Chem.* **28,** 3 (1991) and succeeding articles in that issue.
2. R. C. Haushalter and L. A. Mundi, *Chem. Mater.* **4,** 31 (1992).
3. P. Y. Feng, X. H. Bu, and G. D. Stucky, *J. Solid State Chem.* **129,** 328 (1997).
4. R. A. Laudise, *in* "Crystal Growth: An Introduction" (P. Hartman, Ed.), North-Holland, Amsterdam, 1973.
5. R. F. Belt and J. B. Ings, *J. Crystal Growth* **128,** 956 (1993).
6. G. L. Schimek, W. T. Pennington, P. T. Wood, and J. W. Kolis, *J. Solid State Chem.* **123,** 277 (1996).
7. See for example S. Boudin and K.-H. Lii, *Inorg. Chem.* **37,** 799 (1998).
8. W. T. A. Harrison, M. L. F. Phillips, and G. D. Stucky, *Chem. Mater.* **7,** 1849 (1995).
9. J. R. D. Debord, W. M. Reiff, C. J. Warren, R. C. Haushalter, and J. Zubieta, *Chem. Mater.* **9,** 1994 (1997) and reactions therein.
10. M. B. Korzenski, G. L. Schimek, J. W. Kolis, and G. J. Long, *J. Solid State Chem.* **139,** 152 (1998).
11. M. B. Korzenski and J. W. Kolis, *Chem. Mater.*, submitted.
12. N. Kinomura, N. Matsui, N. Kumada, and F. Muto, *J. Solid State Chem.* **79,** 232 (1989).
13. R. Glaum, R. Gruehn, and M. Moller, *Z. Anorg. Allg. Chem.* **543,** 111 (1986).
14. E. Kostiner and J. R. Rea, *Inorg., Chem.* **13,** 2876 (1974).
15. L. O. Hagman, I. Jansson, and C. Magneli, *Acta Chem. Scand.* **22,** 1419 (1968).
16. W. W. Wendlandt and H. G. Hecht, "Reflectance Spectroscopy." Interscience, New York, 1966.
17. A. C. T. North, D. C. Phillips, and F. S. Mathews, *Acta Crystallogr., Sect. A* **24,** 351 (1968).
18. A. L. Spek, *Acta Crystallogr., Sect. A* **46,** 334 (1990).
19. Y. Lepage, *J. Appl. Crystallogr.* **20,** 264 (1987).
20. G. M. Sheldrick, "SHELXTL-PLUS Crystallographic System, Release 4.11," Siemens Analytical X-Ray Instruments Inc., Madison, WI, 1990.
21. K. H. Lii, P. F. Shih, and T. M. Chen, *Inorg. Chem.* **32,** 4373 (1993).
22. R. D. Shannon, *Acta. Crystallogr., Sect. A* **32,** 751 (1976).
23. K.-H. Lii, P.-F. Shih, and T.-M. Chen, *Inorg. Chem.* **3,** 4373 (1993).
24. K.-H. Lii, T.-Y. Dong, C.-Y. Cheng, and S.-L. Wang, *J. Chem. Soc. Dalton Trans.* 577 (1993).
25. K.-H. Lii, T.-S. Lee, S.-N. Liu, and S.-. Wang, *J. Chem. Soc. Dalton Trans.* 1051 (1993).
26. D. Altermatt and I.D. Brown, *Acta Crystallogr., Sect. B* **41,** 240 (1985).
27. R. A. Nyquist and R. O. Kagel, "Infrared Spectra of Inorganic Compounds," First ed. Academic Press, New York, 1971.
28. S. Khorari, A. Rulmont, and P. Tarte, *J. Solid State Chem.* **131,** 294 (1997).
29. P. Keller and H. Hess, *Neues Jahrbuch Miner., Sect. Mh.* **9,** 395 (1988).
30. I. D. Brown and D. Altermatt, *Acta Crystallogr., Sect. B* **41,** 244 (1985).
31. G. J. Long and C. Gleitzer, *Hyperfine Inter.* **62,** 147 (1990).
32. M. Ijjaali, B. Malaman, G. Venturini, C. Gleitzer, G. J. Long, and F. Grandjean, *J. Phys. Condens. Matter.* **3,** 9597 (1991).
33. B. Malaman, M. Ijjaali, R. Gerardin, G. Venturini, and C. Gleitzer, *Eur. J. Solid State Inorg. Chem.* **29,** 1269 (1992).
34. A. Modaressi, A. Courtois, R. Gerardin, B. Malaman, and C. Gleitzer, *J. Solid State Chem.* **40,** 301 (1981).
35. G. J. Long, A. K. Cheetham, and P. D. Battle, *Inorg. Chem.* **22,** 3012 (1983).
36. P. D. Battle, A. K. Cheetham, C. Gleitzer, W. T. A. Harrison, G. J. Long, and G. Longworth, *J. Phys. C* **15,** L919 (1982).
37. M. Ijjaali, G. Venturini, R. Gerardin, B. Malaman, and C. Gleitzer, *Eur. J. Solid State Inorg. Chem.* **28,** 983 (1991).
38. R. H. Herber, "Chemical Mössbauer Spectroscopy," p. 199. Plenum Press, New York, 1984.
39. J. I. Pankove, "Optical Processes in Semiconductors." Prentice Hall, Englewood Cliffs, NJ, 1971.